IOSR Journal of Engineering (IOSR JEN) **www.iosrjen.org**
ISSN (e): 2250-3021, ISSN (p): 2278-8719
PP 62-67

Effect of Co-substitution on Electrical Behaviour of Nanocrystalline ZnO

Umesh B. Gawas*, R. M. Pednekar
Department of Chemistry, Dnyanprassarak Mandal's College and Research Centre, Assagao, Bardez- Goa, 403507
Email: umeshg29@rediffmail.com *, aryanraj1087@rediffmail.com

Abstract: *ZnO and Co-doped ZnO were successfully synthesized using simple combustion approach. X-ray diffraction studies indicate the monophasic character of the samples and broadness of XRD peaks suggests nanocrystalline nature of ZnO and Co-doped ZnO. The particle size was found to decrease with increasing Co-doping. The FTIR peaks are assigned to the C-O, N-O and O-H stretching in the dry gel, while the IR peaks in the decomposed product are assigned to metal –oxygen stretching vibrations. The room temperature frequency variation of dielectric constant and dielectric loss is explained using Maxwell-Wagner type interfacial polarization and Koop's theory. Ac conductivity increases gradually with frequency upto 10 kHz and then exhibits sharp increase. This conductivity behaviour suggests small polaron hopping type of conduction mechanism. The dc resistivity was found to increase with increasing Co doping in the ZnO. The room temperature low dc resistivity behaviour is attributed to the porous structure and entrapped moisture.*

Keywords: *Nanoparticles, Co-doped ZnO, DC resistivity, combustion synthesis, FTIR spectroscopy.*

I. Introduction

ZnO has received much research attention due to its low toxicity and low price, high chemical and thermal stability, high transparency in the visible wavelength range and unique optical properties. In the powder form, ZnO is a very important material due to its potential applications in numerous areas such as electronics and photonics. ZnO is a very promising photocatalyst for photocatalytic degradation of water pollutants like phenol [1] and its derivatives [2] either under UV light [3] or sunlight [4]. Zinc oxide has been used in numerous applications, such as antireflection coatings, transparent electrodes in solar cells, varistors, light emitting diodes, gas sensors, acousto-optical devices, lasers, near-UV emissions, photocatalysis, antibacterial agents and piezoelectric devices [5]. Zinc oxide (ZnO) is a polar II–VI compound semiconductor whose iconicity resides at the borderline between the covalent and ionic semiconductors. It is an intrinsic n-type semiconductor because of deviation from stoichiometry and the presence of intrinsic defects such as O vacancies (V_O) and Zn interstitials (Zn_i) [6]. ZnO is a semiconductor with wide band gap of 3.37 eV and large exciton binding energy of 60 meV. ZnO is also an environmentally friendly material that does not form toxic byproducts [7]. Nanoparticles(NPs) are essentially a varied form of basic elements derived by altering their atomic and molecular properties. Inorganic NPs, including metal oxides, are promising materials for applications in medicine, such as cell imaging, biosensing, drug/gene delivery, and cancer

therapy[8]–[9]. ZnO NPs belonging to a group of metal oxides are characterized by their photocatalytic and photo-oxidizing ability against chemical and biological species. Doping of semiconductor materials of transition metals is very essential for the application in spintronics. The optical band gap of ZnO nanoparticles was remarkably decreases from 3.32 to 4.12 eV with increase of Co doping levels from 0 to 7 % as revealed from photoluminescence measurements [10]. The antibacterial studies performed against a set of bacterial strains showed that the 2.0 wt% Co-doped ZnO nanoparticles possessed a greater antibacterial effect [11]. The photocatalytic activity of the samples for the removal of methylene blue under visible light irradiation, showed an increase in efficiency from 70% with ZnO to 98% with $Zn_{0.97}Co_{0.03}O$ samples after 150 min of irradiation [12].

II. Experimental

A. Synthesis

All the reagent used were analytical grade and employed in the synthesis without further purification. The sucrose to nitrate ratio (S/N) was calculated by using the oxidizing and reducing valencies of the metal nitrates and sucrose ($C_{12}H_{22}O_{11}$), respectively [13]. Stoichiometric quantity of zinc nitrate was dissolved in water. To this solution stoichiometric quantity of cobalt nitrate (in case of Co-doped ZnO) and sucrose was added. The mixture was evaporated carefully at slow heating rate using hot plate. The gel obtained after the evaporation was dried in oven and ignited at 350^{o}C for 20 minutes using muffle furnace. The sucrose-nitrate mixture froths and finally ignites leaving ultrafine metal oxide powder as residue.

B. Characterization

The structure and phase purity of $Zn_{1-x}Co_xO$ (x = 0.0, 0.02, 0.04, 0.06, 0.08) was determined using X-ray diffractometer (Rigaku Ultima-IV) with Cu K_α radiations through Ni filter. The lattice parameters (a) and (c) were calculated using Bragg's relation [14]. The average crystallite sizes (D) were calculated by Debye-Scherrer formula using most intense XRD peaks. The infrared spectral analysis of samples was carried out using infrared spectrophotometer (Shimadzu FTIR- IR AFFINITY-1). The as obtained powders were pelletized under pressure of 6 ton / inch^2 using hydraulic press and heated at 400^{o}C for 5h. The capacitance of ferrite pellets was measured at different frequencies from 100 Hz to 1 MHz using LCR meter (WAYNE KERR 6500P) at room temperature. The dc resistivity of the pellets of dimension 10mm x 2mm were measured using two probe method.

III. Results And Discussion

A. Structure AND Phase Identification

Fig. 1 shows the XRD patterns of pure and Co-doped ZnO. The XRD peaks indicate that the synthesized samples consist of particles in nanoscale range. The diffraction studies confirmed that the synthesized material was ZnO with wurtzite structure and the entire diffraction peak agreed with the reported JCPDS data (Card No. 36-1451). No additional peaks were observed other than the characteristic peaks for pure ZnO.

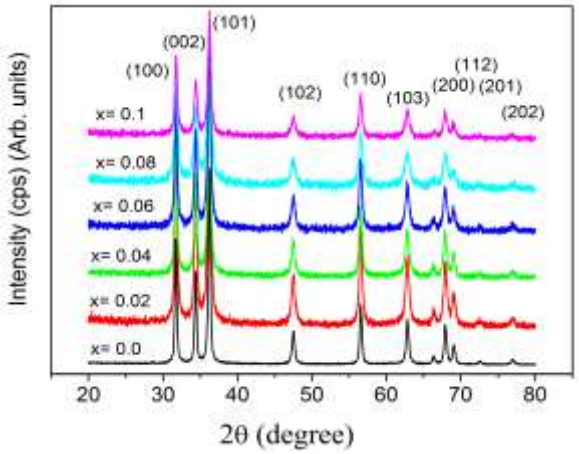

Fig.1. X-ray diffraction pattern of ZnO and Co-doped ZnO

As the dopant concentration increased, the lattice constants changed slightly, and these changes were not proportional. The lattice constants of the doped ZnO samples are comparable to those of undoped ZnO [15]. The aspect ratio (c/a) is nearly constant for all the samples and is well correlated with the ratio of the undoped ZnO sample. These results suggest that the dopant atoms are incorporated in the ZnO lattices with little or no effect on the overall crystal structure. The average crystallite size of the ZnO and Co-doped ZnO samples was found to be in the range 28.7-16.4nm. It was observed that the particle size decreases with increasing dopant concentration.

TABLE I CRYSTAL LATTICE PARAMETER and PARTICLE SIZE of ZnO and Co-DOPED ZnO

x	$a_{(100)}$	$c_{(002)}$	c / a	Average particle size (nm)
0.0	3.251	5.207	1.602	28.7
0.02	3.251	5.197	1.599	18.9
0.04	3.249	5.211	1.604	21.9
0.06	3.251	5.215	1.604	19.4
0.08	3.251	5.211	1.603	16.4
0.1	3.249	5.211	1.604	18.1

B. Ftir Spectroscopic Measurements

The FTIR spectra of the sucrose nitrate gel obtained after drying is shown in the Fig. 2. The broad peak in higher energy region at 3740-3000 cm^{-1} is due to O-H stretching. The broad peak in the region 1630-1340 cm^{-1} is due to N-O stretching as well as C-O stretching. The IR peak in region 480-460 cm^{-1} can be accounted for the metal oxygen stretching. The FTIR spectra of the ZnO and Co-doped ZnO are shown in Fig. 3. The FTIR band in the region 600-400 cm^{-1} is assigned to the Zn^{2+}----O^{2-} and Co^{+2}---O^{2-} stretching vibrations in the hexagonal ZnO structure. The small shift in the position of the band with Co doping can be associated with changes in bond length due to the partial substitution of Co^{+2} ions at the ZnO lattice. The broad absorption peak at 3438 cm^{-1} can be attributed to the characteristic absorption of hydroxyl [16].

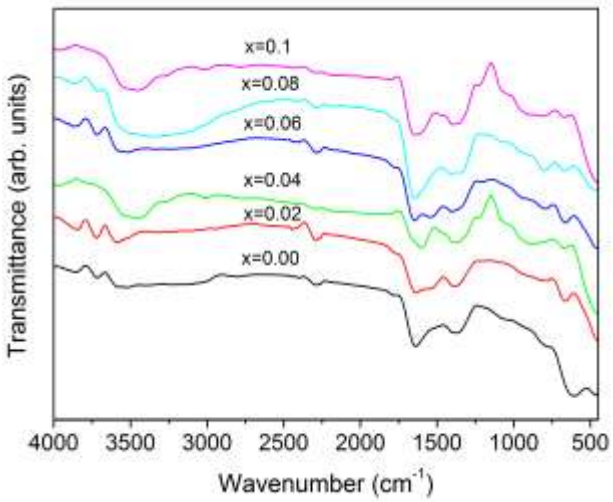

Fig.2. FTIR spectra of crude product of decomposition

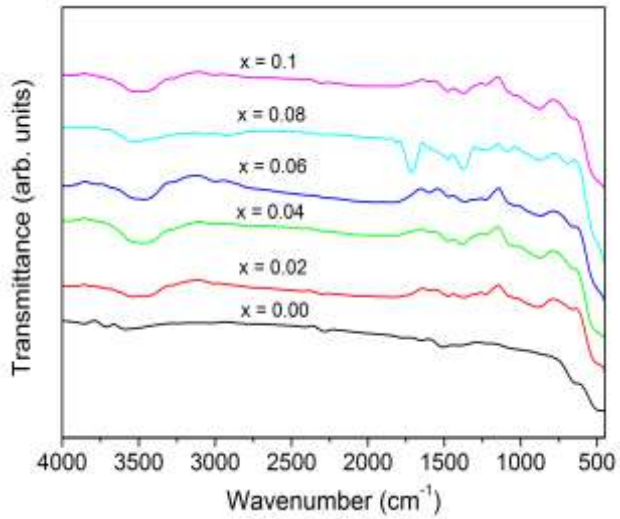

Fig.3. FTIR spectra of Co-doped ZnO

C. Dielectric Measurements

The variation of the dielectric constant with log frequency at room temperatures is shown in Fig.4. The dielectric constant of all the samples found decreases with increasing frequency. This can be explained on the basis of Maxwell-Wagner model which is a result of the inhomogeneous medium of two-layer dielectric structure. In this model, dielectric structure is composed of well conducting grains, which are separated by the poorly conducting grain boundaries [17]. By hopping, electrons can accumulate at grain boundaries due to high resistance and produce polarization. As the frequency of the external electric field increases the hopping frequency of electrons cannot follow the alternating field. This decreases the probability of electron reaching the grain boundary and as a result polarization decreases. The results are in good agreement with the Koops phenomenological theory [18]. The observed higher value of dielectric constant at lower frequency is due to space charge polarization. While at higher frequency, polarization will lags behind the applied field and hence decreases the value of dielectric constant. The dielectric constant increases initially with increasing doping upto 0.04 mol % and then decreases with further increase in Co content.

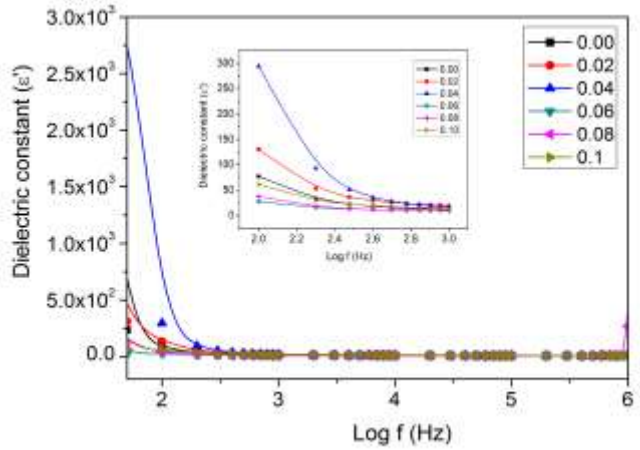

Fig. 4. Frequency variation of dielectric constant

The frequency variation of dielectric loss at room temperature is represented in the Fig. 5. Dielectric loss decreases with increase in frequency and becomes constant at higher frequencies. Dielectric loss arises when the polarization lags behind the applied field and is caused by grain boundaries, impurities and imperfection in the crystal lattice [19]. When the frequency of the applied AC electric field is smaller than the hopping frequency of electrons between Zn^{2+} and Co^{3+} ions, the electrons follow the field and hence the loss is maximum. At higher frequencies of the applied electric field, the hopping frequency of the electron exchange between these ions cannot follow the applied field beyond certain critical frequency and the loss is minimum. The lower value of tan δ (10^{-2}) was observed in the higher frequency range (1MHz) shows that the material is less lossy. The variation of dielectric loss with composition follows same trend as that of dielectric constant upto 1 MHz and then increases sharply.

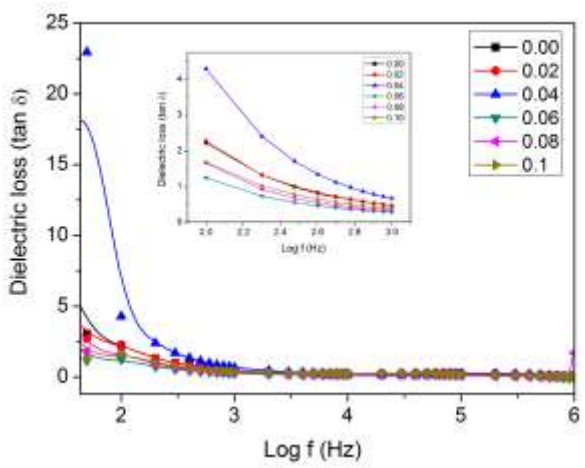

Fig.5. Frequency variation of dielectric loss

The conduction mechanism was determined from the AC conductivity measurement. The variation of AC electrical conductivity (σ_{ac}) with log frequency at room temperature is shown in Fig. 6. The AC conductivity increases gradually with frequency upto 10 KHz and then increases exponentially. At lower frequency, poorly conducting boundaries become more active. As a result hopping frequency between charge carriers decreases. This in turn decreases the conductivity value of the material. As frequency increases, the hopping increases which results in the increase of AC conductivity value for all the samples. A close relationship between tan δ and conductivity was observed. The increase of conductivity is accompanied by an increase of the eddy current which in turn increases the energy loss tan δ [20].

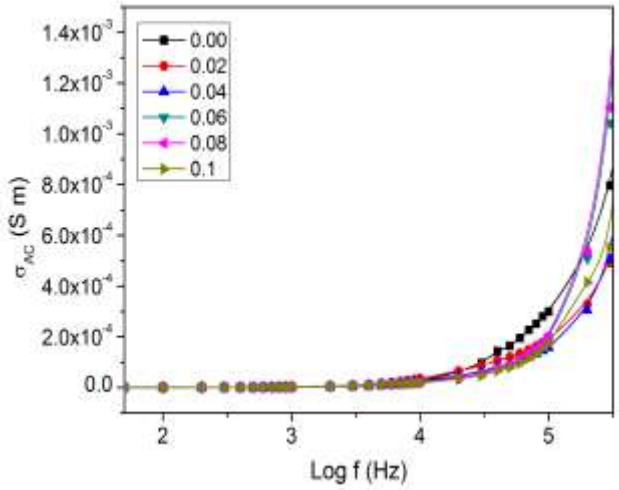

Fig.6. Frequency variation of AC conductivity

D. Dc Resistivity Measurement

The temperature dependence of the dc resistivity (log ρ) is shown in Fig.7. Increase in resistivity with increase in doping concentration of cobalt in ZnO was observed for the doped samples [21, 22]. This resistivity behavior is attributed to the increased defect scattering due to the addition of Co^{2+} ions. Free electrons from the donor levels are trapped by the divalent ions, resulting in the decrease in n-type donor carrier concentration and increase in resistivity. The small amount of cobalt within soluble limit depresses the carrier concentration making the ZnO higher resistive [23]. Critical nature of resistivity evident in the magnetic based semiconductors was attributed to distribution of carriers through exchange interaction [24].

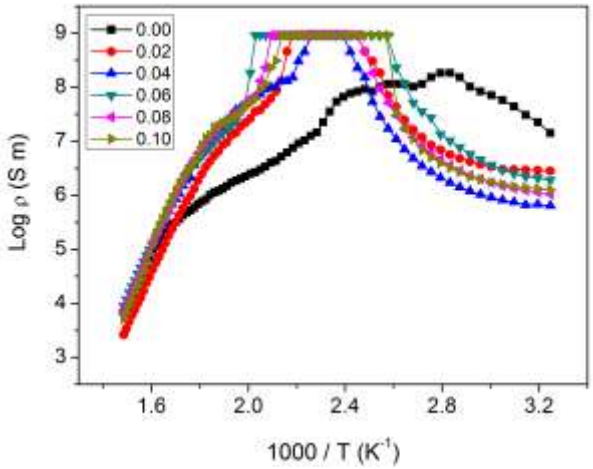

Fig.7. Temperature variation of DC resistivity

Fig.7 shows the observed values of resistivity which decreases slowly with increase of temperature above 393 K for increase in cobalt doping concentration. Substitution of Co^{2+} ions in Zn^{2+} lattice site is expected to create certain oxygen vacancies or zinc interstitials. These vacancies can perform as donors as well as deform the lattice structure to maintain the charge neutrality. The variation in conductivity is also dependent on thermal energy and charge carrier mobility.

IV. Conclusions

The XRD measurements confirmed formation of monophasic character of ZnO as well as Co-doped ZnO. The broadness of the XRD peaks indicates their nanosize nature. The average crystallite size of the ZnO and Co-doped ZnO samples was found to be in the range 28.7-16.4nm and the particle size decreases with increasing Co doping. The lattice constants and aspect ratio of the doped ZnO samples are comparable to those of undoped ZnO. The FTIR spectra of dry sucrose-nitrate gel exhibits the peaks which corresponds to the C-O stretching, N-O stretching as well as O-H stretching due to the sucrose and metal nitrates. The IR peaks observed in the spectra of ZnO and Co-doped ZnO is attributed to the Zn-O as well as Co-O stretching

vibrations. The dielectric constant of all the samples found to decrease with increasing frequency. The dielectric constant increases initially with increasing doping upto 0.04 mol % and then decreases with further increase in Co content. The lower value of tan δ was observed in the higher frequency range (1 MHz) shows that the material is less lossy. The increase of conductivity is accompanied by an increase of the eddy current which in turn increases the energy loss tan δ. The AC conductivity behavior can be correlated to dielectric loss. The dc resistivity was found to increase with increasing Co content. This resistivity behavior is attributed to the increased defect scattering due to the addition of Co^{2+} ions. The room temperature dc resistivity values in the range 10^6 Ωm to 10^7 Ωm suggest the protonic conduction at room temperature due to moisture trapped inside the porous structure of the nanosize oxides.

Acknowledgement

Authors are thankful to the Research Centre, Dnyanprassarak Mandal's College for financial support (DNY/CC/2014-15/03/1198). We would like to thank Mr. Girish Prabhu, Technical Officer, National Institute Oceanography, Donapaula-Goa for XRD measurements.

References

[1]. K. Hayat, M.A. Gondal, M.M. Khaled, S. Ahmed, and A.M. Shemsi, "Nano ZnO synthesis by modified sol gel method and its application in heterogeneous photocatalytic removal of phenol from water", *Appl. Catal. A-Gen*., vol. 393, pp. 122-129, Feb. 2011.

[2]. S. Anandan, A. Vinu, T. Mori, N. Gokulakrishnan, P. Srinivasu, V. Murugesan and K. Ariga, "Photocatalytic Degradation of 2,4,6-Trichlorophenol Using Lanthanum Doped ZnO in Aqueous Suspension", *Catal. Comm.*, vol. 8, No. 9, pp. 1377-1382, Sept. 2007.

[3]. H. Yan, J. Hou, Z. Fu, B. Yang, P. Yang, K. Liu, M. Wen, Y. Chen, S. Fu, and F. Li, "Growth and photocatalytic properties of one-dimensional ZnO nanostructures prepared by thermal evaporation", *Mater. Res. Bull*, vol. 44, pp. 1954-1959, Oct. 2009.

[4]. S. K. Pardeshi, and A.B. Patil, "Solar photocatalytic degradation of resorcinol a model endocrine disrupter in water using zinc oxide", *J. Hazard. Mater*., vol. 163, pp. 403-409, April 2009.

[5]. M. Rezapour, and N. Talebian, "Comparison of structural, optical properties and photocatalytic activity of ZnO with different morphologies: Effect of synthesis methods and reaction media", *Mater. Chem. Phys*., vol. 129, pp. 249-255, Sept. 2011.

[6]. H. Morkoc, U. Ozgur, *Zinc oxide: Fundamentals, Materials and Device Technology*, Wiley, Germany 2009.

[7]. H. Hidaka, K. Nohara, K. Ooishi, J. Zhao, N. Serpone, and E. Pelizzetti, "Photodegradation of surfactants. XV: Formation of SO_4^{2-} ions in the photooxidation of sulfur-containing surfactants" *Chemosphere*, vol. 29, pp. 2619-2624, Dec. 1994.

[8]. L. Wang, Y. Liu, W. Li, X. Jiang, Y. Ji, X. Wu , *et al*. "Selective targeting of gold nanorods at the mitochondria of cancer cells: implications for cancer therapy", *Nano Lett*., vol. 11, pp. 772-780, Feb. 2011.

[9]. Y.N. Wu, D. H. Chen, X. Y. Shi, C. C. Lian, T. Y. Wang, C. S. Yeh, *et al*., "Cancer-cell-specific cytotoxicity of non-oxidized iron elements in iron core-gold shell NPs", *Nanomedicine: NBM*, vol. 7, pp. 420-427, Aug. 2011.

[10]. T. M. Hammad, J. K. Salem, and R. G. Harrison, "Structure, optical properties and synthesis of Co-doped ZnO superstructures", *Applied Nanoscience*, vol. 3, pp. 133-139, April 2013.

[11]. N. M. Basith, J. J. Vijaya, L. J. Kennedy, M. Bououdina, S. Jenefar, and V. Kaviyarasan, "Co-Doped ZnO Nanoparticles: Structural, Morphological, Optical, Magnetic and Antibacterial Studies", *J. Mater. Sci. Tech*., vol. 30, pp. 1108-1117, July 2014.

[12]. N. X. Dung, L. T. Hung ,S. Schulze, M. Hietschold , H. Podlesak, and B. Wielage, "Synthesis, characterization and photocatalytic activity of Co-doped ZnO nanoparticles", *Int. J. Nanotech*., vol. 12, pp. 416- 425, March 2015.

[13]. K. C. Patil, S. T. Aruna, and S. Ekambaram, "Combustion Synthesis", *Current Opinion Sol. State Mater. Sci*., vol. 2, pp.158-165, April 1997.

[14]. B. D. Cullity, "*Elements of X-ray Diffractions"*, Addison Wesley Pub. Co. Inc. 1956.

[15]. S.P. Prakoso, and R. Saleh,"Synthesis and Spectroscopic Characterization of Undoped Nanocrytalline ZnO Particles Prepared by Co-Precipitation,"*Materials Sciences Applications*, vol. 3, pp. 530-537, July 2012.

[16]. A. Kaschner, U. Haboeck, M. Strassburg, G. Kaczmarczyk, A. Hoffmann, C. Thomsen, A. Zeuner, H. R. Alves, D. M. Hofmann, and B. K. Meyer, "Nitrogen-related local vibrational modes in ZnO:N", *Appl. Phys. Lett*., vol. 80, pp. 1909-1911, Jan. 2002.

[17]. A. Thakur, P. Mathur, and M. Singh, "Study of dielectric behaviour of Mn-Zn nano ferrites", *J. Phys. Chem. Sol*., vol. 68, pp. 378-381, March 2007.

[18]. C. G. Koops, "On the Dispersion of Resistivity and Dielectric Constant of Some Semiconductors at Audiofrequencies" *Phys. Rev*., vol. 83, pp. 121-124, July 1951.

[19]. R. V. Mangalaraja, P. Manohar, and F. D. Gnanam, "Electrical and magnetic properties of $Ni_{0.8}Zn_{0.2}Fe_2O_4$/silica composite prepared by sol-gel method", *J. Mater. Sci*., vol. 39, pp-2037-2042, March 2004.

[20]. A. A. Satter, and A. R. Samy, "Dielectric Properties of Rare Earth Substituted Cu-Zn Ferrites", *Physica Status Solidi(a)*, vol. 200, pp. 415-422, Nov. 2003.

[21]. C. Fitzgerald, M. Venkatesan, J. Lunney, L. Dorneles, and J. Coey, "Cobalt-doped ZnO- a room temperature dilute magnetic semiconductor", *Appl. Surf. Sci*., vol. 247, pp. 493-496, July 2005.

[22]. R.B. Kale and C.D. Lokhande, "Room temperature deposition of ZnSe thin films by successive ionic layer adsorption and reaction (SILAR) method" *Mater. Res. Bull*., vol. 39, pp. 1829-1839, Oct. 2004.

[23]. J. Han, P.Q. Mantas and A.M.R. Senos, "Defect chemistry and electrical characteristics of undoped and Mn-doped ZnO", *J. Eur Ceram. Soc*., vol. 22, pp. 49-59, Jan. 2002.

[24]. F. Matsukura, H. Ohno, A. Shen and Y. Sugawara, "Transport properties and origin of ferromagnetism in (Ga,Mn)As", *Phys. Rev.B*, vol. 57, pp. R2037, Jan. 1998.

[25]. S. A. Saafan, T. M. Meaz, E. H. El-Ghazzawy, M. K. El-Nimr, M. M. Ayad and M. Bakr, "A.C. and D.C. conductivity of NiZn ferrite nanoparticles in wet and dry conditions", *J. Magn. Magn. Mater*. vol. 322, pp. 2369-2374, August 2010.

[26]. P. P. Sarangi, S.R. Vadera, M.K. Patra and N.N. Ghosh, "Synthesis and characterization of pure single phase Ni–Zn ferrite nanopowders by oxalate based precursor method", *Powder Tech*., vol. 203, pp. 348-353, Nov. 2010.

[27]. A. Verma, T.C. Goel, R.G. Mendiratta and R.G. Gupta, "High-resistivity nickel-zinc ferrites by the citrate precursor method", *J. Magn. Magn. Mater*., vol. 192, pp. 271-276, Feb. 1999.